SIMULATION OF RF ANALOG CIRCUITS: A SYSTEMATIC EXPOSITION OF THE HARMONIC BALANCE AND COMPLEX ENVELOPE METHODS

Leonardo da Cunha Brito and Paulo Henrique Portela de Carvalho

Resumo - Hoje em dia, a utilização de ferramentas de simulação no projeto de circuitos de RF é indispensável. Dentre as ferramentas mais eficientes, estão aquelas que implementam os algoritmos de simulação denominados método do Equilíbrio Harmônico (ou Harmonic Balance) e método das Envoltórias Complexas (ou Envoltórias Não-lineares, ou Envoltórias Transitórias ou, na língua inglesa, Complex Envelopes). Estas técnicas permitem realizar simulações eficientes e precisas das medidas típicas de RF, possibilitando assim uma redução no número de iterações necessárias no projeto de circuitos, visto que o processo de prototipação pode ser otimizado. Neste artigo, apresentam-se as sistematizações dos métodos do Equilíbrio Harmônico e das Envoltórias Complexas. Adicionalmente, descrevem-se suas características e limitações. Desenvolvem-se as equações básicas dos métodos de simulação, bem como, apresentam-se procedimentos eficientes e robustos para a resolução das equações. Este trabalho tem o propósito de servir como um tutorial para a implementação destes dois métodos de simulação de circuitos.

Palavras-chave: Simulação de circuitos de RF, Harmonic Balance, Complex Envelopes.

Abstract - Nowadays, the use of simulation tools in the design of RF circuits is essential. Among the most efficient tools are those that implement the simulation methods called Harmonic Balance and Complex Envelopes. These techniques allow accurate and efficient simulations of common RF measurements in such a way that the number of design iterations is reduced, given that the prototyping process is optimized. This article has as objectives to present the systematization of those methods and to describe their features and limitations. The basic equations and the algorithms used to solve them are developed. This work is supposed to serve as a tutorial for implementation of these circuit simulation methods.

Keywords: RF circuit simulation, Harmonic Balance, Complex Envelopes.

1. INTRODUCTION

There are three important reasons that sustain the use of CAD tools in the design of RF circuits: to understand the physics of the device composed by interacting elements, to test new concepts, and to optimize projects. Currently, the personal communication market is growing towards the implementation of complete systems built into single chips. Only a small section of the system operates at radio frequencies (RF). However, this is a critical section in the design of communication systems [1]-[2]. Because of the signal frequencies and circuit time-constants, and the performance measurements required, simulators such as SPICE [3] are unsuitable due the necessity to simulate long transients, which would be very time-consuming. SPICE-like simulators implements time domain integration methods. Because of this drawback, special methods have been developed in order to supply the requirements of RF designers. Especially in the last two decades, RF simulation tools have been significantly evolving. Among the most efficient RF simulation methods, are the well-known Harmonic Balance (HB) and the Complex Envelopes (CE). These methods allow simulations of typical RF measurements such as adjacent channel power, DC to RF conversion efficiency, power added efficiency, signal-to-noise ratio, AM/AM and AM/PM conversion, among others. The HB method allows the computation of the steady-state response of a nonlinear circuit excited by one or more tones, whereas the CE method handles multitone circuits (circuits excited by modulating and carrier signals). These two methods represent efficient tools for the design of analog components of communication circuits.

In section 2, the formulations of the HB and CE methods are systematically presented. In the same section, examples illustrate some applications of the methods. Finally, a short discussion and some conclusions are presented in section 4.

2. SYSTEMATIZATION OF THE SIMULATION METHODS

2.1 HARMONIC BALANCE

The Harmonic Balance (HB) is an extensively explored very well established method. There is a vast literature about this technique (see [4]-[6], for instance). The HB simulation provides the steady-state response of stable nonlinear electric circuits. This method is applied to the analysis of distortion and transfer characteristics of amplifiers, mixers, oscillators and other active devices.

In this method, the circuit equation (or nodal equation) is given in the frequency domain ω as

$$\mathbf{Y}(\omega)\mathbf{U}(\omega)+\mathbf{N}(\omega)+\mathbf{W}(\omega)=0 \qquad (1)$$

governed by

Leonardo da C. Brito is with Universidade Federal de Goiás, Goiânia, GO, Brazil. Paulo H. P. de Carvalho is with Universidade de Brasília, Brasília, DF, Brazil.
E-mails: {lcbrito,paulo}@ene.unb.br. Review coordinated by Denise Consonni (Area Editor). Manuscript received Dec/09/2003, reviewed Feb/25/2004, accepted Feb/26/2004.

$$\mathbf{W}(\omega) = \mathrm{F}\{\mathbf{w}(t)\} = \mathrm{F}\left\{\boldsymbol{\varnothing}\left[\mathrm{F}^{-1}\{\mathbf{L}(\omega)\mathbf{X}(\omega)\}\right]\right\} \quad (2)$$

where F designates the multidimensional Fourier transform, $\mathbf{L}(\omega)$ is the derivative and delay operator defined in the frequency domain, and $\boldsymbol{\varnothing}$ defines the behavior of the nonlinear elements. $\mathbf{N}(\omega)$, $\mathbf{X}(\omega)$, $\mathbf{W}(\omega)$, and $\mathbf{U}(\omega)$ are, respectively, vectors with the Fourier coefficients of independent sources $\mathbf{n}(t)$, independent variables (or unknowns) $\mathbf{x}(t)$ controlling $\mathbf{w}(t)$, nonlinear sources $\mathbf{w}(t)$, and potentials $\mathbf{u}(t)$ at the nodes of the circuit. $\mathbf{Y}(\omega)$ is the admittance matrix that characterizes the linear part of the circuit. Equation (1) is generally built by inspection from the Kirchhoff's laws and element's laws. Elements in $\mathbf{w}(t)$ may be voltages, currents, charges and fluxes, as well as their differentiated and delayed versions. In this formulation, for simplicity of exposition, but without loss of generality, we assume that $\mathbf{w}(t)$ refers only to nonlinear current sources. Hence, $\mathbf{w}(t)$ is a vector of nonlinear current sources expressed by

$$\mathbf{w}(t) = \boldsymbol{\varnothing}\left(\mathbf{x}(t), \frac{d\mathbf{x}(t)}{dt}, \mathrm{K}, \frac{d^n\mathbf{x}(t)}{dt^n}, \mathbf{x}_D(t)\right) \quad (3)$$

where $\mathbf{x}_D(t)$ is a vector composed by the delayed version of the voltages $\mathbf{x}(t)$ (each component presents its respective delay). Generally, nonlinear elements are better modeled in the time domain in terms of currents and voltages, as expressed in (3).

As known, electric signals of a circuit can be expressed by their truncated complex Fourier series as

$$\mathbf{n}(t) = \sum_{k=-H}^{H} \mathbf{N}_k\, e^{j\Omega_k t},\ \mathbf{x}(t) = \sum_{k=-H}^{H} \mathbf{X}_k\, e^{j\Omega_k t},$$
$$\mathbf{w}(t) = \sum_{k=-H}^{H} \mathbf{W}_k\, e^{j\Omega_k t},\ \text{and}\ \mathbf{u}(t) = \sum_{k=-H}^{H} \mathbf{U}_k e^{j\Omega_k t} \quad (4)$$

where Ω_k is one of the linear combinations of the fundamental frequencies of the signals in the steady-state regime. That is, Ω_k is a generic frequency of the intermodulation vector

$$\tilde{\mathbf{U}} = \tilde{\mathbf{I}}\ \tilde{\mathbf{u}} \quad (5)$$

where $\tilde{\mathbf{u}} = [\omega_1\ \omega_2\ \Lambda\ \omega_K]^T$ is the base of fundamental frequencies with dimension K and $\mathbf{M} = [\mathbf{m}_{-H}\ \mathbf{m}_{-H+1}\ \Lambda\ \mathbf{m}_H]^T$ is such that $\mathbf{m}_k = [m_{k,1}\ m_{k,2}\ \Lambda\ m_{k,K}]$, with $m_{k,i} \in Z$ such that $\sum_{i=1}^{K} |m_{k,i}| \le NL$ and $|m_{k,i}| \le H_i$, for $i = 1, \mathrm{K}, K$. The value of H_i, for $i = 1, \mathrm{K}, K$, is the truncation order of the Fourier series relative to the fundamental frequency ω_i, and it is also called order of nonlinearity. The value NL is called the global order of nonlinearity of the circuit and it is given by $NL = \max_{i=1,\mathrm{K},K}(H_i)$. Therefore, expression (1) can take the following shape

$$\mathbf{Y}(\Omega_k)\,\mathbf{U}_k + \mathbf{N}_k + \mathbf{W}_k(\mathbf{LX}) = 0 \quad (6)$$

for all Ω_k of the intermodulation frequencies vector. It must be seen that the coefficients of the vector $\mathbf{W}_k(\mathbf{LX})$ are dependent of all the coefficients present in the vector of unknowns $\mathbf{X} = [\mathbf{X}_{-H}\ \mathbf{X}_{-H+1}\ \Lambda\ \mathbf{X}_H]^T$. Moreover, we have that $\mathbf{X}_k = \mathbf{A}_k\mathbf{U}_k$, where $\mathbf{A}_k$ is the incidence matrix related to Ω_k.

Expression (6) can be suitably written in a matrix form as

$$\begin{bmatrix} \mathbf{E}_{-H}(\mathbf{X}) \\ \mathbf{E}_{-H+1}(\mathbf{X}) \\ \mathrm{M} \\ \mathbf{E}_H(\mathbf{X}) \end{bmatrix} = \begin{bmatrix} \mathbf{Y}(\Omega_{-H}) & & & \mathbf{0} \\ & \mathbf{Y}(\Omega_{-H+1}) & & \\ & & \mathrm{O} & \\ \mathbf{0} & & & \mathbf{Y}(\Omega_H) \end{bmatrix} \begin{bmatrix} \mathbf{U}_{-H} \\ \mathbf{U}_{-H+1} \\ \mathrm{M} \\ \mathbf{U}_H \end{bmatrix} + \begin{bmatrix} \mathbf{N}_{-H} \\ \mathbf{N}_{-H+1} \\ \mathrm{M} \\ \mathbf{N}_H \end{bmatrix} + \begin{bmatrix} \mathbf{W}_{-H}(\mathbf{LX}) \\ \mathbf{W}_{-H+1}(\mathbf{LX}) \\ \mathrm{M} \\ \mathbf{W}_H(\mathbf{LX}) \end{bmatrix} \quad (7)$$

with

$$\mathbf{L} = diag(\mathbf{L}(\Omega_{-H}), \mathbf{L}(\Omega_{-H+1}), \mathrm{K}, \mathbf{L}(\Omega_H)) \quad (8)$$

Additionally, we have that $\mathbf{X} = \mathbf{AU}$, where $\mathbf{A} = diag(\mathbf{A}_{-H}, \mathbf{A}_{-H+1}, \mathrm{K}, \mathbf{A}_H)$.

Therefore, in order to find the steady-state response of a nonlinear circuit, we must solve the algebraic nonlinear system (7), which can be represented by

$$\mathbf{E}(\mathbf{X}) = \mathbf{YU} + \mathbf{N} + \mathbf{W}(\mathbf{LX}) = 0 \quad (9)$$

System (9) is commonly solved by an iterative Newton-Raphson procedure with analytical computation of the jacobian. The direct and inverse Fourier transforms are performed by the fast Fourier transforms (FFTs).

At each iteration, the Newton-Raphson procedure offers the following estimate

$$\mathbf{X}^{(i+1)} = \mathbf{X}^{(i)} - \mathbf{J}\left(\mathbf{X}^{(i)}\right)^{-1}\mathbf{E}\left(\mathbf{X}^{(i)}\right) \quad (10)$$

The jacobian is given by

$$\mathbf{J}\left(\mathbf{X}^{(i)}\right)=\frac{d\,\mathbf{E}\left(\mathbf{X}^{(i)}\right)}{d\,\mathbf{X}}=\mathbf{Y}\frac{d\,\mathbf{U}\left(\mathbf{X}^{(i)}\right)}{d\,\mathbf{X}}+\frac{d\,\mathbf{W}\left(\mathbf{L}\mathbf{X}^{(i)}\right)}{d\,(\mathbf{L}\mathbf{X})}\mathbf{L} \quad (11)$$

where $d\,\mathbf{U}\left(\mathbf{X}^{(i)}\right)/d\,\mathbf{X}=\mathbf{A}$.

The derivative $d\,\mathbf{W}\left(\mathbf{L}\mathbf{X}^{(i)}\right)/d\,(\mathbf{L}\mathbf{X})$ is calculated through the following expression

$$\frac{d\,\mathbf{W}\left(\mathbf{L}\mathbf{X}^{(i)}\right)}{d\,(\mathbf{L}\mathbf{X})}= =\begin{bmatrix} \dfrac{d\,\mathbf{W}_{-H}\left(\mathbf{L}\mathbf{X}^{(i)}\right)}{d\,\left(\mathbf{L}(\Omega_{-H})\mathbf{X}_{-H}\right)} & \mathbf{L} & \dfrac{d\,\mathbf{W}_{-H}\left(\mathbf{L}\mathbf{X}^{(i)}\right)}{d\,\left(\mathbf{L}(\Omega_{H})\mathbf{X}_{H}\right)} \\ \mathbf{M} & \mathbf{O} & \mathbf{M} \\ \dfrac{d\,\mathbf{W}_{H}\left(\mathbf{L}\mathbf{X}^{(i)}\right)}{d\,\left(\mathbf{L}(\Omega_{-H})\mathbf{X}_{-H}\right)} & \mathbf{L} & \dfrac{d\,\mathbf{W}_{H}\left(\mathbf{L}\mathbf{X}^{(i)}\right)}{d\,\left(\mathbf{L}(\Omega_{H})\mathbf{X}_{H}\right)} \end{bmatrix} \quad (12)$$

with

$$\frac{d\,\mathbf{W}_{u}\left(\mathbf{L}\mathbf{X}^{(i)}\right)}{d\,\left(\mathbf{L}(\Omega_{v})\mathbf{X}_{v}\right)}=\mathrm{F}\left\{\boldsymbol{\varnothing}'\left[\sum_{k=-H}^{H}\mathbf{L}\mathbf{X}^{(i)}e^{jk\Omega_{1}t}\right]\right\}_{\omega_{u}-\omega_{v}} \quad (13)$$

where $\mathrm{F}\{\cdot\}_{\omega_{u}-\omega_{v}}$ is the spectral component at frequency $\omega_{u}-\omega_{v}$ of the argument. This component results from the operation of the direct Fourier transform. $\boldsymbol{\varnothing}'$ is the vector composed by the derivatives of the nonlinear functions related to the control signals. It must be seen that these signals suffer the action of their respective linear operators.

It is noticeable that all electric signals of the circuit can be obtained by direct manipulation of the equation system (9) if the vector $\mathbf{X}^{(i)}$ is known. Furthermore, a zero vector is commonly used as the initial estimate $\mathbf{X}^{(0)}$ of the Newton-Raphson procedure.

In order to improve the convergence capability of procedure described above, continuation techniques are commonly used. The most used one is that where the levels of the excitation sources of the circuit are varied by a controlling parameter μ. As a result, expression (9) is rewritten as

$$\mathbf{E}(\mathbf{X},\mu)=\mathbf{Y}\mathbf{U}+\mu\mathbf{N}+\mathbf{W}(\mathbf{L}\mathbf{X})=\mathbf{0} \quad (14)$$

where $0<\mu\le 1$, and $\mu=1$ when we have the desired excitation levels.

When the solution of equation (10) $\mathbf{X}_{l}^{(*)}$ is achieved (for excitation levels $\mu_{l}\mathbf{N}$), the continuation solution consists of determining the initial estimate for the $l+1$ step trough the tangent of the solution curve $\mu\times X$. Then,

$$\mathbf{X}_{l+1}^{(0)}=\mathbf{X}_{l}^{(*)}+\Delta\mathbf{X}_{l} \quad (15)$$

where $\Delta\mathbf{X}_{l}$ is the solution of the following system

$$\mathbf{J}\left(\mathbf{X}_{l}^{(*)}\right)\Delta\mathbf{X}_{l}=\frac{\partial\mathbf{E}\left(\mathbf{X}_{l}^{(*)},\mu_{l}\right)}{\partial\mu}\Delta\mu=\mathbf{N}\,\Delta\mu \quad (16)$$

in which $\Delta\mu=\mu_{l+1}-\mu_{l}$.

Starting from the initial estimate $\mathbf{X}_{l+1}^{(0)}$, the solution $\mathbf{X}_{l+1}^{(*)}$ of the balance equation (10) is searched by the Newton-Raphson method. The process is repeated until $\mu=1$, when the final solution by the HB method is obtained.

2.2 HARMONIC BALANCE – ILLUSTRATIVE EXAMPLES

As an example, the equation of the HB method is applied to the illustrative circuit shown in Fig. 1. This circuit presents two current-type nonlinearities, i_1 and i_2, dependent of $v_1(t)$ and of the delayed version $v_2(t-\tau)$ of $v_2(t)$, respectively.

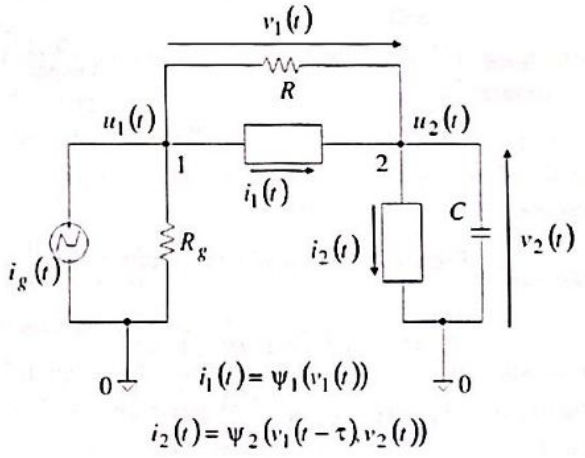

Figure 1. Circuit with two nonlinear current sources.

Equation (17) expresses the HB equation (6) when applied to the circuit of Fig. 1. Node "0" is the reference node.

$$\begin{bmatrix} R_{g}^{-1}+R^{-1} & -R^{-1} \\ -R^{-1} & R^{-1}+j\Omega_{k}C \end{bmatrix}\begin{bmatrix} U_{1k} \\ U_{2k} \end{bmatrix}+ \begin{bmatrix} -I_{gk} \\ 0 \end{bmatrix}+\begin{bmatrix} -I_{1k} \\ I_{1k}-I_{2k} \end{bmatrix}=\begin{bmatrix} 0 \\ 0 \end{bmatrix} \quad (17)$$

with

$$I_{1k}=\mathrm{F}\left\{\psi_{1}\left(\sum_{p=-H}^{H}V_{1p}^{L}e^{jk\Omega_{1}t}\right)\right\}_{\Omega_{k}}$$
$$I_{2k}=\mathrm{F}\left\{\psi_{2}\left(\sum_{p=-H}^{H}V_{2p}^{L}e^{jk\Omega_{1}t}\right)\right\}_{\Omega_{k}} \quad (18)$$

and

$$\begin{bmatrix} V_{1k} \\ V_{2k} \end{bmatrix}=\begin{bmatrix} 1 & -1 \\ 0 & 1 \end{bmatrix}\begin{bmatrix} U_{1k} \\ U_{2k} \end{bmatrix}=\mathbf{A}_{k}\begin{bmatrix} U_{1k} \\ U_{2k} \end{bmatrix}$$
$$\begin{bmatrix} V_{1k}^{L} \\ V_{2k}^{L} \end{bmatrix}=\begin{bmatrix} 1 & 0 \\ 0 & e^{-jk\Omega_{1}\tau} \end{bmatrix}\begin{bmatrix} V_{1k} \\ V_{2k} \end{bmatrix}=\mathbf{L}(\Omega_{k})\begin{bmatrix} V_{1k} \\ V_{2k} \end{bmatrix} \quad (19)$$

The steady-state response of the circuit is achieved when the balance between expressions (17) and (18) are obtained for all frequencies of the intermodulation vector $\hat{\mathbf{U}}$.

As a second example, the HB method was applied in the simulation of the 4.0GHz FET nonlinear amplifier shown in Fig. 2. The graphic of Fig. 4 show the results obtained by the input power sweep from -5 to 25dBm. Fig. 3 exhibits the equivalent circuit model of the FET. It is a modified Tajima model [5]. The functions that describe the behavior of the sources I_{GS}, Q_{GS}, I_{GD}, and I_{DS} are given, respectively, by equations (20), (21), (22), and (23). It can be noticed that the voltages V_{GS} and V_{DS} are the control variables of the nonlinear sources. The values of the circuit parameters are also shown in Fig. 3.

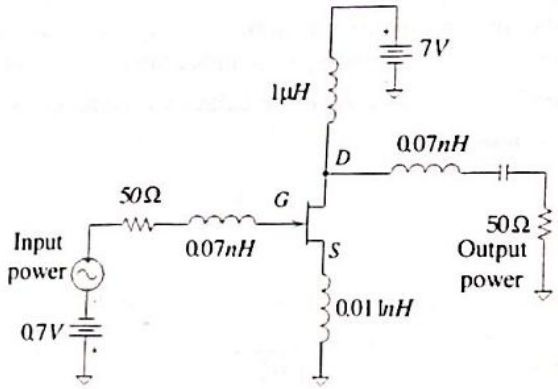

Figure 2. FET nonlinear amplifier.

$$I_{GS}(V_{GS}) = I_s\left[\exp(\alpha V_{GS}) - 1\right] \tag{20}$$

$$Q_{GS}(V_{GS}) = Q_0\left(\frac{1 - V_{GS}}{V_{bi}}\right)^{0.5} \tag{21}$$

$$I_{GD}(V_{GS}, V_{DS}) = I_a\left(a + bV_{DS}^{e}\right)^{(c - dV_{GS})} \tag{22}$$

$$I_{DS}(V_{GS}, V_{DS}) = I_{dss} F_G F_D$$

$$F_G = \frac{1}{K}\left[V_{gsn} - \frac{1 - \exp(-mV_{gsn})}{m}\right]$$

$$F_D = 1 - \exp\left[-\left(V_{dsn} + aV_{dsn}^2 + bV_{dsn}^3\right)\right]$$

$$V_{gsn} = 1 + \frac{V_{gs}(t-\tau)}{V_p} \tag{23}$$

$$V_{dsn} = \frac{V_{ds}}{V_{dsp}\left(1 + \frac{wV_{gs}(t-\tau)}{V_p}\right)}$$

$$V_p = V_{p0} + pV_{DS} + V_{phi}$$

$$K = 1 - \frac{1 - \exp(-m)}{m}$$

In Fig. 4, we can see the quasi-linear behavior of the amplifier when it is excited by power levels lower than 10dBm. The harmonic distortion effects are stronger for excitation levels higher than 10dBm (high power harmonic components).

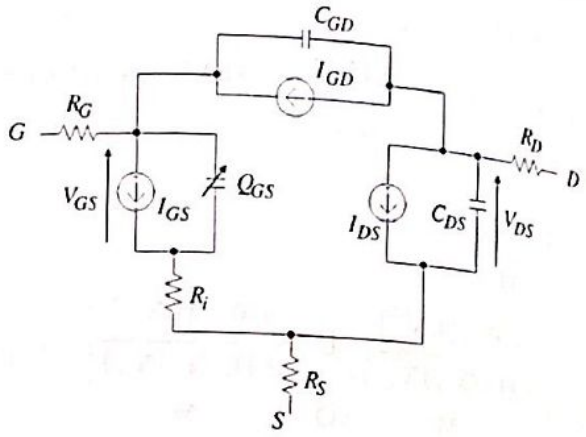

$R_G = 0.26\Omega$ $R_S = 0.26\Omega$ $C_{GD} = 0.153\,pF$ $\tau = 4.0\,ps$
$R_D = 0.2\Omega$ $R_i = 0.15\Omega$ $C_{DS} = 0.530\,pF$

I_{GS}: $I_S = 0.2\,\mu A$ $\alpha = 18$

Q_{GS}: $Q_0 = -4.992\,pC$ $V_{bi} = 0.8V$

I_{GD}: $I_a = 0.3\,\mu A$ $a = 1.2$ $b = 0.06$ $c = 5.0$ $d = 0.81$ $e = 1.36$

I_{DS}: $I_{dss} = 0.6402\,A$ $V_{p0} = 2.399V$ $V_{dsp} = 0.8964V$ $V_{phi} = 0.2695V$
$a = 1.062$ $b = 0.01939$ $m = 3.2521$ $p = 0.2574$ $w = 0.829$

Figure 3. FET equivalent circuit model.

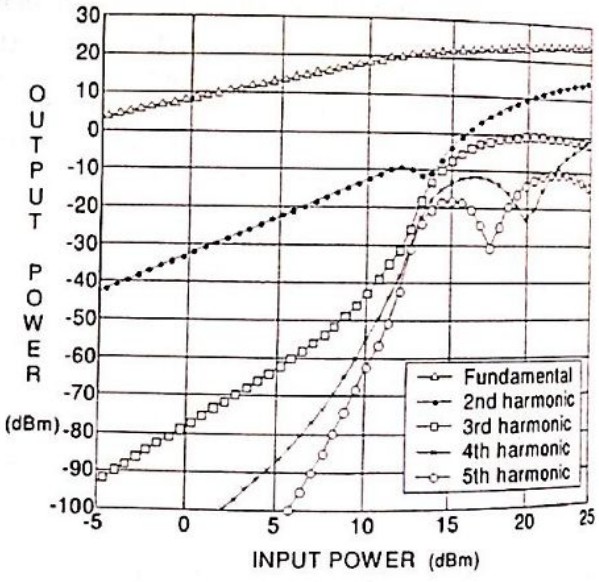

Figure 4. Nonlinear amplifier response curves.

2.3 COMPLEX ENVELOPES

The Complex Envelopes (CE) method [7]-[10] is also a mixed time/frequency approach, but it is capable to provide efficiently the transient response of the circuit. When applying this method, we assume that the electric signals of the circuit have low and high frequency components, like those signals present into RF communication circuits. This method is inherently more efficient than the traditional time-domain simulation methods (time integration methods)

when the circuit presents the feature mentioned above. In this case, the method offers a high gain in terms of demanded time and computation resources.

In order to develop clearly the formulation of the CE method, we assume, without loss of generality, that the electric signals of the circuit are written as

$$s(t)=\sum_{k_0=-N_0}^{N_0}\left(\frac{1}{2\pi}\int_{-W/2}^{W/2}S(k_0\omega_0+\Omega)e^{j\Omega t}d\Omega\right)e^{jk_0\omega_0 t} \qquad (24)$$

in which each spectral component $S(k_0\omega_0+\Omega)$ is positioned at frequency $k_0\omega_0+\Omega$, where $k_0\omega_0$ is the k_0-th harmonic frequency of the carrier ω_0. This expression can be obtained from the inverse Fourier transform applied to a signal which frequency spectrum presents the shape shown in Fig. 5. Fig. 5(a) depicts the typical shape of an analog or digitally modulated carrier. When this type of signal feeds a nonlinear circuit, electric signals described by equation (24) are generated, as sketched in Fig. 5(b). They present harmonic distortions and intermodulation products inside their frequency bands. We consider only one carrier, but this formulation can be easily extended to the case of multiple carriers by simply considering in (17) all intermodulation products of all carrier frequencies and their harmonics, instead of considering only one carrier and its harmonics.

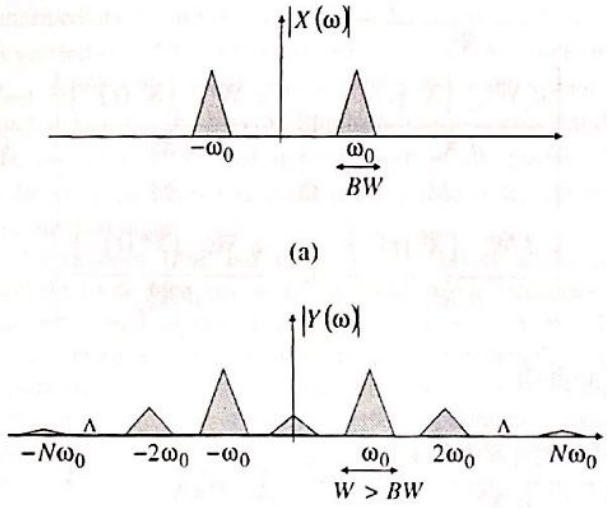

Figure 5. Frequency spectra (absolute values): (a) modulated carrier, (b) distortion and intermodulation.

Equation (24) can be rewritten as

$$s(t)=\sum_{k_0=-N_0}^{N_0}\mathcal{S}_{k_0}(t)e^{jk_0\omega_0 t} \qquad (25)$$

where

$$\mathcal{S}_{k_0}(t)=\frac{1}{2\pi}\int_{-W/2}^{W/2}S(k_0\omega_0+\Omega)e^{j\Omega t}d\Omega \qquad (26)$$

Equations (25) and (26) represent a decomposition of the modulated signal $s(t)$ in a finite number of bands around the carrier and its harmonics. Then, expression (25) is signal composed by high frequency, $\exp(jk_0\omega_0 t)$, and low frequency components, $\mathcal{S}_{k_0}(t)$. Equation (26) is the complex envelope (or time-varying Fourier components) of $s(t)$ at frequency $k_0\omega_0$. According to the sampling theorem, it is necessary to sample $s(t)$ with a rate equals or superior to $2(N_0\omega_0+W/2)$ so that the signal can be correctly reconstructed. On the other hand, the components $\mathcal{S}_{k_0}(t)$ must be sampled with a rate considerably lower, given by W. We generally have that $W/2<<\omega_0$ in real-world systems. It can also be noticed that we can know $s(t)$ taking into account only the time series of its complex envelopes, since the components $\exp(jk_0\omega_0 t)$ are known. As a result, we can reconstruct $s(t)$ with the samples of the envelopes $\mathcal{S}_{k_0}(t)$ sampled with rate W, in the following way

1. By interpolation, we take the values of the complex envelopes $\mathcal{S}_{k_0}(t)$ at the time instants starting from the time origin and obeying the sampling rate $2(N_0\omega_0+W/2)$.

2. Then, we apply the interpolated values to (26). It must be noticed that the components $\exp(jk_0\omega_0 t)$ are known at each time instant.

Therefore, we can reconstruct the fast signal $s(t)$ taking into account the much slower signals $\mathcal{S}_{k_0}(t)$.

Taking into account the procedure described above, it is desired to characterize the behavior of the electric circuit by an equation whose solution is the set of the complex envelopes of the signals, since the high frequency components are known a priori. Equation (1) is used for this purpose. If we approximate the transfer function of the circuit, say, make a first order Taylor series expansion with the admittance matrix $\mathbf{Y}(\omega)$ around $k_0\omega_0$, we obtain

$$\begin{aligned}&\left[\mathbf{Y}(k_0\omega_0)+\Omega\mathbf{Y}'(k_0\omega_0)\right]\mathbf{U}(k_0\omega_0+\Omega)\\&+\mathbf{N}(k_0\omega_0+\Omega)+\mathbf{W}(k_0\omega_0+\Omega)=\mathbf{0}\end{aligned} \qquad (27)$$

And then, if we apply the inverse Fourier transform in (19), in terms of Ω, in each term of the sum of (27), we obtain

$$\begin{aligned}&\mathbf{Y}(k_0\omega_0)\,\mathcal{U}_{k_0}(t)+\mathcal{Y}_{k_0}'\frac{d}{dt}\mathcal{U}_{k_0}(t)\\&+\mathcal{N}_{k_0}(t)+\mathcal{W}_{k_0}(t)=\mathbf{0}\end{aligned} \qquad (28)$$

for $k_0=-N_0,-N_0+1,\ldots,N_0$. It can be verified that $\mathcal{Y}_{k_0}'$ is the derivative of $\mathbf{Y}(\omega)$ in terms of ω evaluated at $k_0\omega_0$ an multiplied by $-j$, that is, $\mathcal{Y}_{k_0}'=-j\,d\,\mathbf{Y}(k_0\omega_0)/d\omega$.

The first order approximation applied is adequate for modeling linear elements (dispersive or not) if the condition

$W/2 << \omega_0$ is verified, as in the cases of commercial communication circuits.

From (28), we can obtain the values of the unknowns using expression $\tilde{\mathbf{X}}_{k_0}(t) = \mathbf{A}_{k_0}\tilde{\mathbf{U}}_{k_0}(t)$, in which $\mathbf{A}_{k_0}$ is the incidence matrix of the control variables at $k_0\omega_0$. The nonlinear sources vector $\tilde{\mathbf{W}}_{k_0}(t)$ is a function of the commands $\tilde{\mathbf{X}}_{p_0}(t) = \mathbf{L}(p_0\dot{\mathbf{U}}_0)\,\tilde{\mathbf{X}}_{p_0}(t) + \mathbf{E}_{p_0}\dfrac{d}{dt}\tilde{\mathbf{X}}_{p_0}(t)$, with $p_0 = -N_0, -N_0+1, \mathrm{K}, N_0$. The same development applied to $\mathbf{Y}(\omega)$ and $\mathbf{U}(\omega)$ is also applied to $\mathbf{L}(\omega)$ and $\mathbf{X}(\omega)$. Then, $\mathbf{E}_{p_0} = -j\,d\,\mathbf{L}(p_0\omega_0)/d\omega$.

Additionally, from (28) we have

$$\tilde{\mathbf{W}}_{k_0}(t) = F_{\tau_c}\left\{\boldsymbol{\varnothing}\left[\sum_{p_0=-N_0}^{N_0}\tilde{\mathbf{X}}_{p_0}^{L}(t)e^{jp\omega_0\tau_c}\right]\right\}_{k_0\omega_0} \tag{29}$$

and $F_{\tau_c}\{\cdot\}_{k_0\omega_0}$ is the component of the argument at $k_0\omega_0$ calculated by the Fourier transform along the time axis τ_c of the carrier.

Expression (28) can also be written in matrix notation as

$$\begin{bmatrix}\tilde{\mathbf{E}}_{-N_0}(\tilde{\mathbf{X}}(t))\\ \tilde{\mathbf{E}}_{-N_0+1}(\tilde{\mathbf{X}}(t))\\ \mathrm{M}\\ \tilde{\mathbf{E}}_{N_0}(\tilde{\mathbf{X}}(t))\end{bmatrix} = \begin{bmatrix}\mathbf{Y}(-N_0\dot{\mathbf{U}}_0) & & & \mathbf{0}\\ & \mathbf{Y}((-N_0+1)\dot{\mathbf{U}}_0) & & \\ & & \mathrm{O} & \\ \mathbf{0} & & & \mathbf{Y}(N_0\dot{\mathbf{U}}_0)\end{bmatrix}\begin{bmatrix}\tilde{\mathbf{U}}_{-N_0}(t)\\ \tilde{\mathbf{U}}_{-N_0+1}(t)\\ \mathrm{M}\\ \tilde{\mathbf{U}}_{N_0}(t)\end{bmatrix}$$
$$+\begin{bmatrix}\mathbf{Y}_{-N_0} & & & \mathbf{0}\\ & \mathbf{Y}_{-N_0+1} & & \\ & & \mathrm{O} & \\ \mathbf{0} & & & \mathbf{Y}_{N_0}\end{bmatrix}\begin{bmatrix}\tilde{\mathbf{U}}_{-N_0}(t)\\ \tilde{\mathbf{U}}_{-N_0+1}(t)\\ \mathrm{M}\\ \tilde{\mathbf{U}}_{N_0}(t)\end{bmatrix}$$
$$+\begin{bmatrix}\tilde{\mathbf{N}}_{-N_0}(t)\\ \tilde{\mathbf{N}}_{-N_0+1}(t)\\ \mathrm{M}\\ \tilde{\mathbf{N}}_{N_0}(t)\end{bmatrix}+\begin{bmatrix}\tilde{\mathbf{W}}_{-N_0}(\tilde{\mathbf{X}}(t))\\ \tilde{\mathbf{W}}_{-N_0+1}(\tilde{\mathbf{X}}(t))\\ \\ \tilde{\mathbf{W}}_{N_0}(\tilde{\mathbf{X}}(t))\end{bmatrix} \tag{30}$$

with $\tilde{\mathbf{X}}(t) = \left[\tilde{\mathbf{X}}_{-N_0}(t)\;\; \tilde{\mathbf{X}}_{-N_0+1}\;\; \mathrm{L}\;\; \tilde{\mathbf{X}}_{N_0}\right]^T$ and $\tilde{\mathbf{X}}(t) = \left[\tilde{\mathbf{X}}_{-N_0}(t)\;\; \tilde{\mathbf{X}}_{-N_0+1}(t)\;\; \mathrm{L}\;\; \tilde{\mathbf{X}}_{N_0}(t)\right]^T$.

Consequently, the algebraic system to be solved, related to (30), is given by

$$\tilde{\mathbf{E}}(\tilde{\mathbf{X}}(t)) = \mathbf{Y}\dot{\tilde{\mathbf{U}}}(t) + \tilde{\mathbf{Y}}\tilde{\mathbf{U}}(t) + \tilde{\mathbf{N}}(t) + \tilde{\mathbf{W}}(\tilde{\mathbf{X}}(t)) = \mathbf{0} \tag{31}$$

In (24), we have that $\dot{\tilde{\mathbf{X}}}(t) = \mathbf{A}\dot{\tilde{\mathbf{U}}}(t)$, in which $\mathbf{A} = diag\left(\mathbf{A}_{-N_0}, \mathbf{A}_{-N_0+1}, \mathrm{K}, \mathbf{A}_{N_0}\right)$.

The system (31) is also usually solved by a Newton-Raphson algorithm and the Fourier transforms are performed by FFTs.

In this method, at each iteration we have the following estimate

$$\tilde{\mathbf{X}}(t)^{(i+1)} = \tilde{\mathbf{X}}(t)^{(i)} - \mathbf{J}\left(\tilde{\mathbf{X}}(t)^{(i)}\right)^{-1}\tilde{\mathbf{E}}\left(\tilde{\mathbf{X}}(t)^{(i)}\right) \tag{32}$$

and the jacobian is given by

$$\mathbf{J}\left(\tilde{\mathbf{X}}(t)^{(i)}\right) = \frac{d\,\mathbf{E}\left(\tilde{\mathbf{X}}(t)^{(i)}\right)}{d\,\tilde{\mathbf{X}}} = \mathbf{Y}\frac{d\,\tilde{\mathbf{U}}(t)}{d\,\tilde{\mathbf{X}}} + \frac{d\,\tilde{\mathbf{W}}\left(\tilde{\mathbf{X}}(t)^{(i)}\right)}{d\,\tilde{\mathbf{X}}}\mathbf{L} \tag{33}$$

where $d\,\dot{\tilde{\mathbf{U}}}(t)/d\,\dot{\tilde{\mathbf{X}}}$ is equals to $\mathbf{A}$. Additionally, we have that $d\,\tilde{\mathbf{U}}(t)/d\,\dot{\tilde{\mathbf{X}}} = \mathbf{0}$.

The derivative $d\,\tilde{\mathbf{W}}\left(\tilde{\mathbf{X}}(t)^{(i)}\right)/d\,\dot{\tilde{\mathbf{X}}}$ is given by

$$\frac{d\,\tilde{\mathbf{W}}\left(\tilde{\mathbf{X}}(t)^{(i)}\right)}{d\,\dot{\tilde{\mathbf{X}}}} = \begin{bmatrix}\dfrac{d\,\tilde{\mathbf{W}}_{-N_0}\left(\tilde{\mathbf{X}}(t)^{(i)}\right)}{d\,\dot{\tilde{\mathbf{X}}}_{-N_0}} & \mathrm{L} & \dfrac{d\,\tilde{\mathbf{W}}_{-N_0}\left(\tilde{\mathbf{X}}(t)^{(i)}\right)}{d\,\dot{\tilde{\mathbf{X}}}_{N_0}}\\ \mathrm{M} & \mathrm{O} & \mathrm{M}\\ \dfrac{d\,\tilde{\mathbf{W}}_{N_0}\left(\tilde{\mathbf{X}}(t)^{(i)}\right)}{d\,\dot{\tilde{\mathbf{X}}}_{-N_0}} & \mathrm{L} & \dfrac{d\,\tilde{\mathbf{W}}_{N_0}\left(\tilde{\mathbf{X}}(t)^{(i)}\right)}{d\,\dot{\tilde{\mathbf{X}}}_{N_0}}\end{bmatrix} \tag{34}$$

in which

$$\frac{d\,\tilde{\mathbf{W}}_u\left(\tilde{\mathbf{X}}(t)^{(i)}\right)}{d\,\dot{\tilde{\mathbf{X}}}_v} = \mathrm{F}_{\tau_c}\left\{\boldsymbol{\varnothing}'\left[\sum_{p_0=-N_0}^{N_0}\tilde{\mathbf{X}}_{p_0}(t)e^{jp\omega_0\tau_c}\right]\right\}_{\omega_u-\omega_v} \tag{35}$$

where $\mathrm{F}_{\tau_c}\{\cdot\}_{\omega_u-\omega_v}$ is the spectral component of the argument at frequency $\omega_u - \omega_v$ obtained by an application of the Fourier transform on $\boldsymbol{\varnothing}'$, which is a vector composed by the derivatives of the nonlinear functions in terms of the control variables.

Once the numerical solution along the time is necessary, we need to have the discrete-time version of system (31) according to some time integration method. This method must also be applied to the other equations used in the solution process. We chose the Euler implicit method [11] due its numerical stability and ease of implementation. Hence, expression (31) is rewritten as

$$\begin{aligned}&\mathbf{E}\left(\mathbf{X}^{k}(t_s)\right)=\\&\mathbf{Y}\mathbf{U}(t_s)+\mathbf{F}\frac{\mathbf{U}(t_s)-\mathbf{U}(t_{s-1})}{t_s-t_{s-1}}\\&+\mathbf{N}(t_s)+\mathbf{W}\left(\mathbf{X}^{k}(t_s)\right)=\mathbf{0}\end{aligned}\qquad(36)$$

where

$$\mathbf{X}^{k}(t_s)=\mathbf{L}\,\mathbf{X}(t_s)+\mathbf{E}\frac{\mathbf{X}(t_s)-\mathbf{X}(t_{s-1})}{t_s-t_{s-1}}\qquad(37)$$

Once expressions (32) to (35) do not present time differentiations, we only need to consider $t=t_s$.

Usually, zero initial conditions are considered, that is, all electric signals of the circuit are zero in $t=t_{-1}$. Besides that, the solutions obtained in $t=t_{s-1}$ are used as initial estimates in $t=t_s$. That is, $\mathbf{X}(t_s)^{(0)}=\mathbf{X}(t_{s-1})^{(*)}$, where $\mathbf{X}(t_{s-1})^{(*)}$ is the solution of the system in $t=t_{s-1}$. This feature increases the efficiency of the solution algorithm. However, in the case we have abrupt transitions on the envelopes (real and/or imaginary parts) the Newton-Raphson algorithm may fail, given that the previous solution may not be a good estimate for the current time instant. To solve this problem, the following procedure is applied. When the solution in $t=t_{s-1}$ is achieved, we search for the solution in $t=t_s$. If the solution is not obtained due convergence problems, we take a new intermediary t_s in the range t_{s-1} to t_s. Then, a new search is carried out. This process is repeated until the solution in t_{s-1} represents a good estimate for the current instant, in such a way that the Newton-Raphson becomes efficient due the proximity of the solutions of both of the points. The solution in each previous point is used as an initial estimate for the next point.

Expressions (36) and (37) can be solved applying a sampling rate proportional to the width of the sidebands of the modulated signals. This value is given by $W/2$. The time domain integration methods demand a sampling rate drastically higher, which is proportional to the maximum frequency of the band-limited modulated signals $N_0\omega_0+W/2$. That is, the gain in processing time when using the CE method is proportional to $(N_0\omega_0)/(W/2)$. For example, in the simulation of an RF device that has modulating bandwidths of 100kHz and a carrier oscillating at 1GHz, the gain will be about 10^5, in the case that ten harmonics of the carrier frequency are taken into account.

2.4 COMPLEX ENVELOPES – ILLUSTRATIVE EXAMPLES

For the circuit shown in Fig. 1, when we take the expressions of the CE method (36) and (37), we obtain the following representations of the circuit

$$\begin{aligned}&\begin{bmatrix}R_g^{-1}+R^{-1} & -R^{-1}\\ -R^{-1} & R^{-1}+jk_0\omega_0C\end{bmatrix}\begin{bmatrix}\tilde{U}_{1k_0}(t_s)\\ \tilde{U}_{2k_0}(t_s)\end{bmatrix}\\&+\begin{bmatrix}0 & 0\\ 0 & C\end{bmatrix}\begin{bmatrix}\tilde{U}'_{1k_0}(t_s)\\ \tilde{U}'_{2k_0}(t_s)\end{bmatrix}\\&+\begin{bmatrix}-\tilde{I}_{g_{k_0}}(t_s)\\ 0\end{bmatrix}\\&+\begin{bmatrix}-\tilde{I}_{1k_0}(t_s)\\ \tilde{I}_{1k_0}(t_s)-\tilde{I}_{2k_0}(t_s)\end{bmatrix}=\begin{bmatrix}0\\0\end{bmatrix}\end{aligned}\qquad(38)$$

with

$$\begin{aligned}\tilde{I}_{1k_0}(t_s)&=F_{\tau_c}\left\{\psi_1\left(\sum_{p_0=-N_0}^{N_0}\tilde{V}^{L}_{1p_0}(t_s)e^{jp_0\omega_0\tau_c}\right)\right\}_{k_0\omega_0}\\\tilde{I}_{2k_0}(t_s)&=F_{\tau_c}\left\{\psi_2\left(\sum_{p_0=-N_0}^{N_0}\tilde{V}^{L}_{2p_0}(t_s)e^{jp_0\omega_0\tau_c}\right)\right\}_{k_0\omega_0}\end{aligned}\qquad(39)$$

and

$$\begin{aligned}&\begin{bmatrix}\tilde{V}_{1k_0}(t_s)\\ \tilde{V}_{2k_0}(t_s)\end{bmatrix}=\begin{bmatrix}1 & -1\\ 0 & 1\end{bmatrix}\begin{bmatrix}\tilde{U}_{1k_0}(t_s)\\ \tilde{U}_{2k_0}(t_s)\end{bmatrix}=\mathbf{A}_k\begin{bmatrix}\tilde{U}_{1k_0}(t_s)\\ \tilde{U}_{2k_0}(t_s)\end{bmatrix}\\&\begin{bmatrix}\tilde{V}^{L}_{1k_0}(t_s)\\ \tilde{V}^{L}_{2k_0}(t_s)\end{bmatrix}=\begin{bmatrix}1 & 0\\ 0 & e^{-jk_0\omega_0\tau}\end{bmatrix}\begin{bmatrix}\tilde{V}_{1k_0}(t_s)\\ \tilde{V}_{2k_0}(t_s)\end{bmatrix}\\&+\begin{bmatrix}0 & 0\\ 0 & \tau e^{-jk_0\omega_0\tau}\end{bmatrix}\begin{bmatrix}\tilde{V}'_{1k_0}(t_s)\\ \tilde{V}'_{2k_0}(t_s)\end{bmatrix}\\&=\mathbf{L}(k_0\omega_0)\begin{bmatrix}\tilde{V}_{1k_0}(t_s)\\ \tilde{V}_{2k_0}(t_s)\end{bmatrix}+\mathbf{E}_{k_0}\begin{bmatrix}\tilde{V}'_{1k_0}(t_s)\\ \tilde{V}'_{2k_0}(t_s)\end{bmatrix}\end{aligned}\qquad(40)$$

Expressions (38) and (39) define the equations of the CE method and they are solved using the procedure described above.

Finally, in Fig. 7, we can see the result obtained by the application of the CE method to the BJT amplifier of Fig. 6. The graphics show the behaviors of the complex envelopes of the input and output signals from the DC to the third order harmonic. The in-phase (real part) and quadrature (imaginary part) of the envelopes are shown. A 900 MHz carrier modulated by an 8PSK signal at 30kbps excites the amplifier. The 8PSK signal was sampled at 200 kHz, that is, twenty samples per symbol were used.

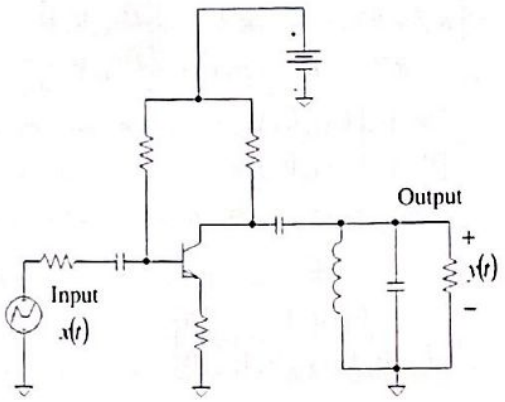

Figure 6. BJT amplifier.

2.5 MAIN FEATURES OF THE METHODS

Among the main features of the HB method, are:

- It is fast and accurate when the electric signals can be approximated by a small number of Fourier coefficients in the steady-state regime.
- Signals must be stable.
- It takes into account the fact that linear lumped and distributed elements are better modeled in the frequency domain and nonlinear elements are better modeled in the time domain.
- Parameter sweep (gain versus power/frequency, for example) can be performed with high efficiency, once the solution for a previous point is commonly a good estimate for the subsequent point, with high probability.

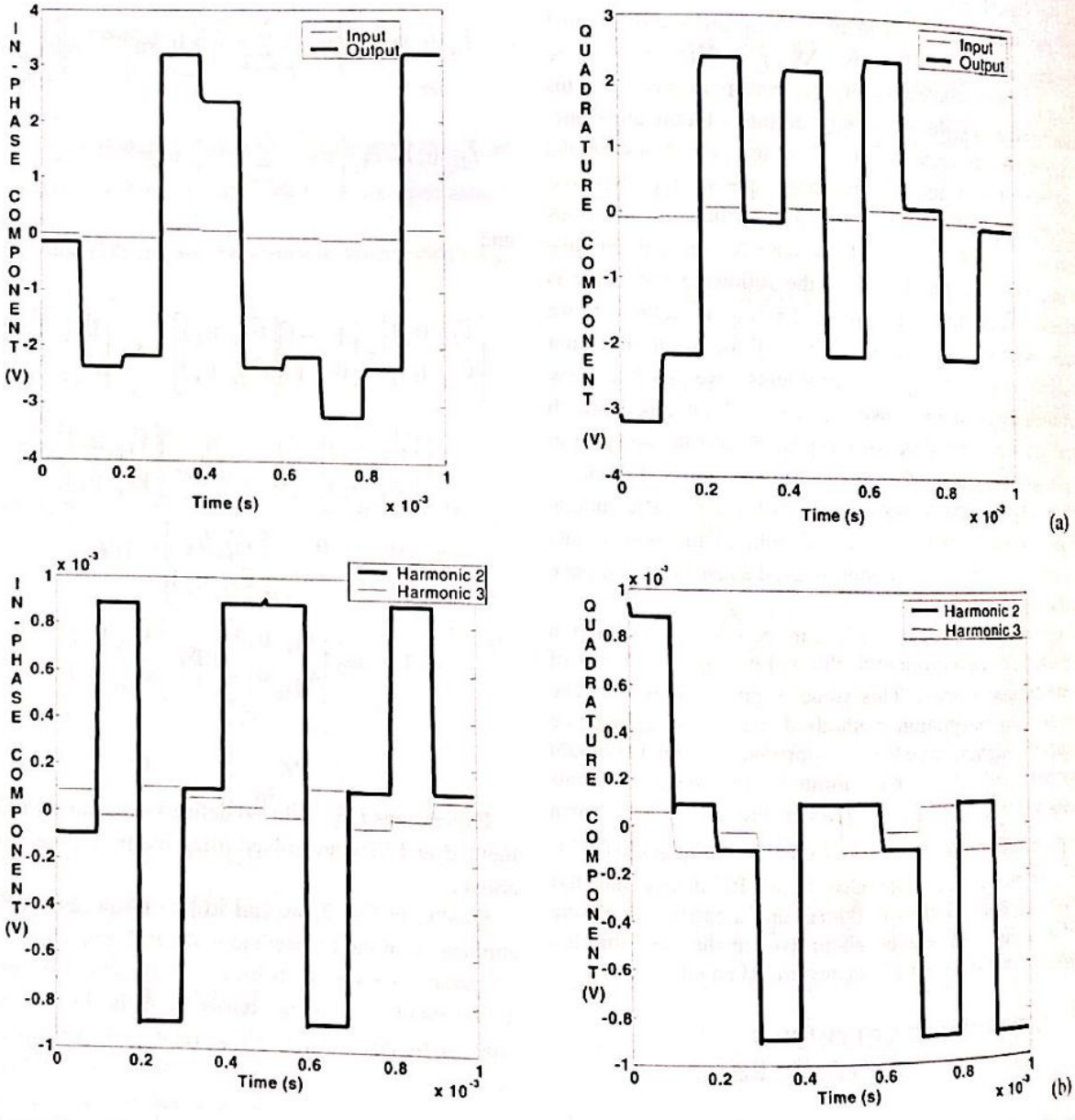

Figure 7. (a) In-phase and quadrature components of the input (thin line) an of the output (thick line); (b) In-phase and quadrature components of second order (thick line) and of third order (thin line). The k_0-th order harmonic of ω_0 is $k_0\omega_0$.

- It offers the steady-state response. Suppressing the transient response is suitable when the circuit provides irrelevant information in this interval, but it is a limitation when we want to analyze the dynamic behavior of the electrical signals (the bit error rate, for example).
- The evaluation of the jacobian demands large amounts of memory and computational processing in the simulation of large circuits. The relevance of this problem was reduced by the use of the Krylov iterative techniques [12], which allow simulation of nonlinear circuits with millions of unknowns and nonlinearities.

The CE method presents the following features:

- It efficiently provides both transient and steady-state responses.
- The electric signals can be stable or unstable.
- This is essentially a multitone method (it works with several fundamental frequencies) due the specific preconditioning of the electric variables. It is able to efficiently work with circuits excited by modulated carriers.
- It demands an amount of computational processing and memory allocation drastically lower than the ones demanded by time integration methods and by the HB method.
- This method is based on an inherent characteristic of communication systems, say, the bandwidths of the baseband signals, as well as the bandwidths of the sidebands of the modulated signals, are relatively much smaller than the carrier frequencies. This characteristic allows the use of the Taylor expansion of the transfer function of the circuit without a significant degradation of numerical accuracy.

Therefore, given the features of the methods, it can be seen that they offer to the designer a good toolbox for the simulation of RF circuits. For example, the designer can obtain the steady-state response, visualize the behavior of the carrier harmonics along the time or verify the spectral regrowth of an RF device.

Appendix A shows the contributions of the basic circuit elements to the circuit equations. Both methods, HB and CE, are considered.

3. CONCLUSIONS

The most efficient approaches currently used in the design of RF communication circuits, the Harmonic Balance and the Complex Envelopes methods, were systematically exposed in this paper. The formulations presented the nonlinear circuit equations as well as the procedures to efficiently and robustly solve the equations. Furthermore, the features (features and limitations) of the methods were listed, as their abilities to handle the simulation of multitone circuits, for example. Finally, some examples indicated the capabilities of both methods.

APPENDIX A

HARMONIC BALANCE

The contributions to the HB equation $\mathbf{Y}(\Omega_k)\mathbf{U}_k + \mathbf{N}_k + \mathbf{W}_k(\mathbf{LX}) = \mathbf{0}$ are as follows. The contributions of the other circuit elements are straightforward to be obtained [11].

ADMITTANCE

Fig. A.1 and equation (A.1) shows the admittance model and its contribution to the HB equation, respectively. V_{pk} and V_{qk} are the voltages in nodes p and q at Ω_k, respectively. The element's law is $I(\omega) = Y(\omega)V(\omega)$, where $I(\omega)$ and $V(\omega)$ are the current and voltage across the element in the frequency domain. Additionally, Y_k is the admittance of the element at Ω_k.

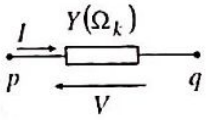

Figure A.1. Admittance model.

$$\begin{array}{c} \\ p \\ q \end{array}\begin{array}{c} \begin{array}{ccccc} p & & q & & \end{array} \\ \begin{bmatrix} \mathrm{M} & & \mathrm{M} & \\ \Lambda & Y_k & \Lambda & -Y_k & \Lambda \\ \mathrm{M} & & \mathrm{M} & \\ \Lambda & -Y_k & \Lambda & Y_k & \Lambda \\ \mathrm{M} & & \mathrm{M} & \end{bmatrix} \\ \mathbf{Y}(\Omega_k) \end{array} \begin{array}{c} \\ \\ \\ \\ \\ \end{array} \begin{array}{c} \\ \begin{bmatrix} \mathrm{M} \\ V_{pk} \\ \mathrm{M} \\ V_{qk} \\ \mathrm{M} \end{bmatrix} \\ \mathbf{U}_k \end{array} \qquad \text{(A.1)}$$

IMPEDANCE

Fig. A.2 and (A.2) respectively shows the impedance model and its contribution to the HB equation. V_{pk} and V_{qk} are the voltages in nodes p and q at Ω_k, respectively. The element's law is $V(\omega) = Z(\omega)I(\omega)$, where $I(\omega)$ and $V(\omega)$ are the current and voltage across the element in the frequency domain. $I(\Omega_k)$ is the current crossing the element at Ω_k. Z_k is the impedance of the element at Ω_k.

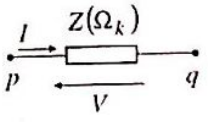

Figure A.2. Impedance model.

$$
\begin{array}{c}
\begin{array}{ccccc} & p & & q & \quad I \end{array} \\
\begin{array}{c} p \\ q \\ I \end{array}
\begin{bmatrix}
 & & & & \mathrm{M} & \\
 & & \Lambda & & 1 & \Lambda \\
 & & & & \mathrm{M} & \\
 & & \Lambda & & -1 & \Lambda \\
 & \mathrm{M} & & \mathrm{M} & & \mathrm{M} \\
\Lambda & 1 & \Lambda & -1 & \Lambda & -Z_k \quad \Lambda \\
 & \mathrm{M} & & \mathrm{M} & & \mathrm{M}
\end{bmatrix}
\begin{bmatrix} \mathrm{M} \\ V_{pk} \\ \mathrm{M} \\ V_{pk} \\ \mathrm{M} \\ I \\ \mathrm{M} \end{bmatrix} \\
\mathbf{Y}(\Omega_k) \qquad\qquad \mathbf{U}_k
\end{array}
\tag{A.2}
$$

CURRENT SOURCE

Fig. A.3 and (A.3) respectively shows the model of the current source and its contribution. The behavior of this element follows $I(\omega) = J(\omega)$. Additionally, $J_k = J(\Omega_k)$.

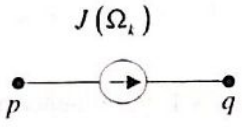

Figure A.3. Current source model.

$$
\begin{array}{c}
\begin{array}{c} \\ p \\ q \end{array}
\begin{bmatrix} \mathrm{M} \\ J_k \\ \mathrm{M} \\ -J_k \\ \mathrm{M} \end{bmatrix} \\
\mathbf{N}_k
\end{array}
\tag{A.3}
$$

VOLTAGE SOURCE

The behavior of this element is given by $V(\omega) = E(\omega)$ and its model and contribution are shown in Fig. A.4 and (A.4), respectively. As can be seen $E_k = E(\Omega_k)$.

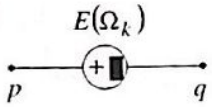

Figure A.4. Voltage source model.

$$
I \begin{bmatrix} \mathrm{M} \\ -E_k \\ \mathrm{M} \end{bmatrix} \text{ and } \mathbf{N}_k
\qquad
\begin{array}{c}
\begin{array}{ccccc} & p & & q & \quad I \end{array} \\
\begin{array}{c} p \\ q \\ I \end{array}
\begin{bmatrix}
 & & & & \mathrm{M} & \\
 & & \Lambda & & 1 & \Lambda \\
 & & & & \mathrm{M} & \\
 & & \Lambda & & -1 & \Lambda \\
 & \mathrm{M} & & \mathrm{M} & & \mathrm{M} \\
\Lambda & 1 & \Lambda & -1 & \Lambda & \\
 & \mathrm{M} & & \mathrm{M} & &
\end{bmatrix}
\begin{bmatrix} \mathrm{M} \\ V_{pk} \\ \mathrm{M} \\ V_{pk} \\ \mathrm{M} \\ I \\ \mathrm{M} \end{bmatrix} \\
\mathbf{Y}(\Omega_k) \qquad\qquad \mathbf{U}_k
\end{array}
\tag{A.4}
$$

VOLTAGE CONTROLLED VOLTAGE SOURCE

Fig. A.5 and (A.5) respectively shows the model and the contribution of the voltage controlled voltage source. The parameter β is the voltage gain.

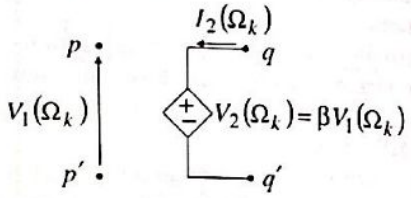

Figure A.5. Voltage controlled voltage source model.

$$
\begin{array}{c}
\begin{array}{ccccccc} & p & & p' & q & q' & \quad I_2 \end{array} \\
\begin{array}{c} p \\ p' \\ q \\ q' \\ I_2 \end{array}
\begin{bmatrix}
 & & & & & & & & & & \mathrm{M} & \\
 & & & & & & & & & & 1 & \Lambda \\
 & & & & & & & & & & \mathrm{M} & \\
 & & & & & & & & & & -1 & \Lambda \\
 & \mathrm{M} & & \mathrm{M} & & \mathrm{M} & & \mathrm{M} & & \mathrm{M} & & \\
\Lambda & -\beta & \Lambda & \beta & \Lambda & 1 & \Lambda & -1 & \Lambda & & & \\
 & \mathrm{M} & & \mathrm{M} & & \mathrm{M} & & \mathrm{M} & & & &
\end{bmatrix}
\begin{bmatrix} \mathrm{M} \\ V_{pk} \\ \mathrm{M} \\ V_{p'k} \\ \mathrm{M} \\ V_{qk} \\ \mathrm{M} \\ V_{q'k} \\ \mathrm{M} \\ I_2 \\ \mathrm{M} \end{bmatrix} \\
\mathbf{Y}(\Omega_k) \qquad\qquad \mathbf{U}_k
\end{array}
\tag{A.5}
$$

VOLTAGE CONTROLLED CURRENT SOURCE

Fig. A.6 and (A.6) shows the model and the contribution of the voltage controlled current source, respectively. The parameter g is the voltage-to-current gain.

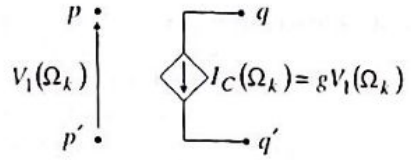

Figure A.6. Voltage controlled current source model.

$$
\begin{array}{c}
\begin{array}{cccccccccccc} & p & & p' & & q & & q' & & I_C & & \end{array} \\
\begin{array}{c} p \\ p' \\ q \\ q' \\ I_C \end{array}
\left[\begin{array}{ccccccccccc}
 & & & & & & & & & & \\
 & & & & & & & & & & \\
 & & & & & & & & M & & \\
 & & & & & & \Lambda & & 1 & \Lambda & \\
 & & & & & & & & M & & \\
 & & & & & & \Lambda & & -1 & \Lambda & \\
 & M & & M & & & & & M & & \\
\Lambda & -g & \Lambda & g & \Lambda & & & \Lambda & 1 & \Lambda & \\
 & M & & M & & & & & M & &
\end{array}\right]
\left[\begin{array}{c} M \\ V_{pk} \\ M \\ V_{p'k} \\ M \\ V_{qk} \\ M \\ V_{q'k} \\ M \\ I_C \\ M \end{array}\right] \\
\mathbf{Y}(\Omega_k) \qquad\qquad \mathbf{U}_k
\end{array}
\tag{A.6}
$$

NONLINEAR CURRENT SOURCE

This element (shown in Fig. A.7) contributes as a current source, as shown in Fig. A.3. But, instead of contributing to $\mathbf{N}_k$, it contributes to $\mathbf{W}_k$. The coefficient $J(\Omega_k)$ can be calculated applying the Fourier transform on the function $j(t)$ that describes the behavior of the source in the time-domain.

$$J(\Omega_k) = F\{j(t)\}_{\Omega_k}$$

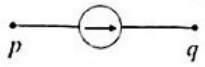

Figure A.7. Nonlinear current source model.

NONLINEAR VOLTAGE SOURCE

This element (shown in Fig. A.8) contributes as a voltage source, as shown in Fig. A.4. It also contributes to $\mathbf{W}_k$. In this case, the coefficient $E(\Omega_k)$ can be calculated applying the Fourier transform on the function $e(t)$ that describes the behavior of the source in the time-domain.

$$E(\Omega_k) = F\{e(t)\}_{\Omega_k}$$

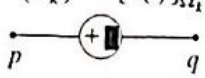

Figure A.8. Nonlinear voltage source model.

COMPLEX ENVELOPES

The contributions of the basic circuit elements to the CE equation can be obtained from their respective contributions to the HB equation. In the CE circuit equation

$$\mathbf{Y}(k_0\dot{\omega}_0)\tilde{\mathbf{U}}_{k_0}(t) + \mathbf{\mathfrak{Y}}_{k_0}\tilde{\mathbf{U}}'_{k_0}(t) + \tilde{\mathbf{N}}_{k_0}(t) + \tilde{\mathbf{W}}_{k_0}(t) = \mathbf{0},$$

only terms related to $\mathbf{\mathfrak{Y}}_{k_0}$ need to be considered here, since $\mathbf{Y}(k_0\dot{\omega}_0)$ is composed by the contributions of the basic elements (HB contributions shown above) evaluated at $\Omega_k = k_0\dot{\omega}_0$. Then, only $\mathbf{\mathfrak{Y}}_{k_0} = -j\,d\,\mathbf{Y}(k_0\omega_0)/d\omega = -j\mathbf{Y}'(k_0\omega_0)$ need to be developed. Nevertheless, it can be noticed that the evaluation of $\mathbf{\mathfrak{Y}}_{k_0}$ is straightforward. For example, the admittance contributes as shown in Fig. A.12. The same procedure can be applied to find the contributions of the other circuit elements.

$$
\begin{array}{c}
\begin{array}{ccccccc} & & p & & & & q \end{array} \\
\begin{array}{c} p \\ q \end{array}
\left[\begin{array}{ccccccc}
 & & M & & & & M \\
\Lambda & & Y_{k_0} & \Lambda & & -Y_{k_0} & \Lambda \\
 & & M & & & & M \\
\Lambda & & -Y_{k_0} & \Lambda & & Y_{k_0} & \Lambda \\
 & & M & & & & M
\end{array}\right]
\left[\begin{array}{c} M \\ \tilde{V}_{pk_0}(t) \\ M \\ \tilde{V}_{qk_0}(t) \\ M \end{array}\right] \\
\mathbf{Y}(k_0\omega_0) \qquad\qquad \tilde{\mathbf{U}}_{k_0}(t)
\end{array}
$$

$$
\begin{array}{c}
\begin{array}{ccccccc} & & p & & & & q \end{array} \\
\begin{array}{c} p \\ q \end{array}
\left[\begin{array}{ccccccc}
 & & M & & & & M \\
\Lambda & & -j\mathfrak{K}_{k_0} & \Lambda & & j\mathfrak{K}_{k_0} & \Lambda \\
 & & M & & & & M \\
\Lambda & & j\mathfrak{K}_{k_0} & \Lambda & & -j\mathfrak{K}_{k_0} & \Lambda \\
 & & M & & & & M
\end{array}\right]
\left[\begin{array}{c} M \\ \tilde{V}'_{pk_0}(t) \\ M \\ \tilde{V}'_{qk_0}(t) \\ M \end{array}\right] \\
\mathbf{\mathfrak{Y}}(k_0\omega_0) \qquad\qquad \tilde{\mathbf{U}}'_{k_0}(t)
\end{array}
\tag{A.7}
$$

REFERENCES

[1] B. Razavi, "Challenges in portable RF transciever design," *IEEE Trans. Circuits and Devices*, Sep. 1996, pp. 12-55.

[2] K. Kundert, "Introduction to RF simulation and its applications," *IEEE Journal of Solid State Circuits*, vol. 34, n. 9, Sep. 1999.

[3] L. Nagel, "SPICE2: A computer program to simulate semiconductor circuits," *Electron. Res. Lab.*, Univ. of California at Berkley, UCB/ERL M520, 1975.

[4] V. Rizzoli, A. Lipparini, A. Costanzo, F. Mastri, C. Cecchetti, A. Neri, and D. Masotti, "State-of-the-art of harmonic balance simulation of forced nonlinear microwave circuits by the piecewise technique," *IEEE Trans. Microwave Theory Tech.*, vol. 40, Jan. 1992, pp. 12–28.

[5] P. Carvalho, *Approche orientée objet de l'analyse des circuits non-linéaires hyperfrequences. Architectures de*

simulateurs et bibliothèques de composants logiciels, Doctoral thesis, Univ. of Limoges, France, 1993.

[6] V. Rizzoli, A. Neri, P. Ghiri, and F. Mastri, "Simulation and design of nonlinear microwave circuits: An overview of techniques for the treatment of oscillators," *Proc. Int. Workshop West German IEEE Chapter*, Oct. 1990, pp. 123–136.

[7] U. L. Rohde and D. P. Newkirk, *RF/Microwave circuit design for wireless applications*, Wiley-Interscience, 2000.

[8] E. Ngoya and R. Lachevèque, "Envelope transient analysis: a new method for the transient and steady state analyis of microwave communication systems and circuits," *IEEE MTT-S Int. Microwave Symp. Dig.*, 1996, pp. 1365-1368.

[9] J. Roychowdhury, "Efficient methods for simulating highly nonlinear multi-rate circuits," *Proc. Design Automation Conf.*, 1997.

[10]L. Brito and P. Carvalho, "EHBSim: Matlab-based nonlinear circuit simulation program (Harmonic Balance and Nonlinear Envelope methods)," *Journal Microwaves and Optoelectron-ics*, vol. 2, Dec. 2001, pp. 1-21.

[11]L. Chua and P. Lin, *Computer-aided analysis of electronic circuits*, Prentice Hall, 1975.

[12]V. Rizzoli, "A Krylov-subspace technique for the simulation of integrated RF/microwave subsystems driven by digitally modulated carriers," *Int. Journal RF Microwave Computer-aided Eng.*, vol. 9, Nov. 1999.

Leonardo da Cunha Brito received the E.E. degree from Universidade Federal de Goiás in 1998. He received the M.S.E.E. and Dr.E.E. degrees from University of Brasília in 2001 and 2002, respectively. He is currently a professor at Escola de Engenharia Elétrica e de Computação, Universidade Federal de Goiás. His areas of interest include modeling methods, numeric simulation and optimization for communication circuits and systems.

Paulo Henrique Portela de Carvalho received the E.E. degree from University of Brasília and the M.S.E.E. and Dr.E.E. degrees from University of Limoges in France, having carried out works at Institut de Recherche en Communications Optiques et Microondes (IRCOM) at Limoges in 1988, 1989 and 1993, respectively. He was a researcher for Centre National de Recherche Scientifique in association with IRCOM. He is currently a professor at Departamento de Engenharia, Universidade de Brasília and his areas of interest include numeric simulation and optimization for circuits and nonlinear communication systems, especially as applied to microwaves, focused on the development of techniques based on Harmonic Balance and Nonlinear Envelope methods and on Evolutionary Algorithms.